

Tunable Signal Processing in Synthetic MAP Kinase Cascades

Ellen C. O'Shaughnessy,¹ Santhosh Palani,² James J. Collins,^{1,4,*} and Casim A. Sarkar^{2,3,*}

¹Howard Hughes Medical Institute and Department of Biomedical Engineering, Center for BioDynamics and Center for Advanced Biotechnology, Boston University, Boston, MA 02215, USA

²Department of Bioengineering

³Department of Chemical and Biomolecular Engineering
University of Pennsylvania, Philadelphia, PA 19104, USA

⁴Wyss Institute for Biologically Inspired Engineering, Harvard University, Boston, MA 02115, USA

*Correspondence: jcollins@bu.edu (J.J.C.), casarkar@seas.upenn.edu (C.A.S.)

DOI 10.1016/j.cell.2010.12.014

SUMMARY

The flexibility of MAPK cascade responses enables regulation of a vast array of cell fate decisions, but elucidating the mechanisms underlying this plasticity is difficult in endogenous signaling networks. We constructed insulated mammalian MAPK cascades in yeast to explore how intrinsic and extrinsic perturbations affect the flexibility of these synthetic signaling modules. Contrary to biphasic dependence on scaffold concentration, we observe monotonic decreases in signal strength as scaffold concentration increases. We find that augmenting the concentration of sequential kinases can enhance ultrasensitivity and lower the activation threshold. Further, integrating negative regulation and concentration variation can decouple ultrasensitivity and threshold from the strength of the response. Computational analyses show that cascading can generate ultrasensitivity and that natural cascades with different kinase concentrations are innately biased toward their distinct activation profiles. This work demonstrates that tunable signal processing is inherent to minimal MAPK modules and elucidates principles for rational design of synthetic signaling systems.

INTRODUCTION

MAPK pathways are ubiquitous, versatile signaling modules found in all eukaryotic cells. They transmit and process signals regulating a broad array of cell fate decisions, including proliferation, differentiation, motility, stress responses, and apoptosis (Avruch, 2007). Though several MAPK families have been elucidated, all consist of three sequential kinases activated by dual, nonprocessive phosphorylation events. The biological design principles underlying a three-tiered cascade structure have been the subject of vigorous debate for many years. A number of hypotheses have been put forth to account for the

use of multistep signaling pathways, including signal amplification, increased signaling speed, multiple points of regulation, noise tolerance, and the generation of switch-like responses (Chen and Thorer, 2005). Though it is likely that this heavily conserved pathway has evolved to serve multiple purposes, its structure clearly enables great flexibility of system response. Extensive experimental work on MAPK cascades has shown that responses can be graded or switch-like (ultrasensitive), transient or sustained, and monostable or bistable (Bhalla et al., 2002; Huang and Ferrell, 1996; Poritz et al., 2001; Santos et al., 2007).

A growing body of research has demonstrated that the systems-level properties of MAPK activation vary greatly depending on cellular context and that the characteristics of this activation can determine cell fate. Seminal work on the activation of p42 MAPK in *X. laevis* demonstrated steep ultrasensitivity (Ferrell and Machleder, 1998; Huang and Ferrell, 1996), whereas studies of MAPK cascades in *S. cerevisiae* revealed graded activation profiles (Poritz et al., 2001). A series of studies in mammalian systems showed that different cell types exhibit either switch-like (Bagowski et al., 2003; Harding et al., 2005) or proportional (Mackeigan et al., 2005; Whitehurst et al., 2004) activation responses. Even within the same cell type, an individual MAPK cascade can exhibit different dynamic responses that lead to distinct cell fates. In PC12 cells, MAPK activation is transient and graded when stimulated with epidermal growth factor, leading to proliferation. In contrast, nerve growth factor stimulation results in cell differentiation through sustained and ultrasensitive MAPK activation (Marshall, 1995). Recent work has shown that altering the activation profile of MAPK in these cells is sufficient to reverse the stimulus-phenotype relationship (Santos et al., 2007). Further, in BHK cells, tethering the MAPK module to the plasma membrane can lower the threshold of activation, and consequently, the percentage of cells that differentiate depends upon both the stimulus magnitude and the location of the cascade in the cell (Harding et al., 2005). Finally, it has been shown that activation of MAPK in NIH 3T3 fibroblasts is dependent upon temporal dynamics of the stimulus (Bhalla et al., 2002). Naive cells exhibit bistable MAPK activation in response to platelet-derived growth factor, whereas previously stimulated cells show proportional, monotonic activation. It has been proposed

that this desensitization enables the downregulation of MAPK activity, a molecule whose prolonged stimulation can be deleterious.

It is clear from both experimental and theoretical work that the behavior of MAPK cascades in vivo is dictated, in part, by multiple levels of feedback regulation. In particular, bistability, an essential characteristic in many cell fate decisions, arises through feedback. However, feedback alone is not sufficient to achieve bistability. Bistable responses require a nonlinearity in the system, feedback to reinforce the nonlinearity, and proper balance between the system components (Ferrell and Xiong, 2001). Ultrasensitivity in MAPK activation is a critical, systems-level property, as it can serve as the fundamental nonlinearity required to achieve stable, potentially irreversible cellular decisions. Indeed, several experimental studies of bistable MAPK activation report ultrasensitive activation profiles as well (Bhalla et al., 2002; Ferrell and Machleder, 1998; Santos et al., 2007). Dissecting the contributions of ultrasensitivity and feedback to a specific bistable response is often untenable in the context of complex endogenous signaling networks.

Many biological systems are organized into functional modules that perform key steps in a larger process (Hartwell et al., 1999). It is often difficult to characterize the potential behaviors of these component subsystems in vivo because of interconnectivity and complex layers of regulation found in biological systems. This is particularly true in signaling networks, which exhibit multifaceted regulation such as feedback, localization, and extensive, functional crosstalk (Natarajan et al., 2006). Nonetheless, interpreting, influencing, and predicting how complex networks carry out biological functions depends critically upon our understanding of their component modules. Here, we use a synthetic biology approach to obviate the challenges of interconnectivity in uncovering the inherent capabilities of the MAPK module; we do so by systematically applying intrinsic and extrinsic perturbations to tune the activation dynamics of a minimal, well-insulated cascade. By studying an isolated module, we develop a mechanistic understanding of the effects of these perturbations both experimentally and computationally.

In the present study, we built an exogenous, minimal MAPK cascade to investigate the effects of extrinsic and intrinsic regulators on the plasticity of this isolated signaling module. We expressed the mammalian Raf-MEK-ERK cascade in the yeast *S. cerevisiae* and applied the intrinsic perturbation of concentration variation between cascade members and the extrinsic perturbations of scaffolding and negative regulation. We show that varying the relative concentrations of MEK and ERK confers great flexibility of the system response and may prime the cascade for either low or high ultrasensitivity. Strikingly, the *X. laevis* p42 MAPK cascade that shows sharp ultrasensitivity and the *S. cerevisiae* pheromone pathway that is more graded both fit well within the theoretical framework generated by this intrinsic perturbation. In addition, we identify cascading itself as a concentration-dependent mechanism for generating ultrasensitivity. We further demonstrate that, in contrast to a biphasic dependence on scaffold concentration (prozone effect), expression of a two-member scaffold results in a monotonic dependence of signal strength on scaffold concentration, with a sharp

reduction observed at high concentration. Finally, introducing negative regulation of either MEK or ERK leads to a reduction in ultrasensitivity and an increase in threshold, even in the absence of feedback. We used a computational model to integrate these intrinsic and extrinsic perturbations over a large parameter space and found regions in which signal characteristics can be tuned independently. Experimentally, we demonstrate the decoupling of signal strength from the ultrasensitivity and threshold of the response. Thus, through the use of a synthetic signaling module, we identified mechanisms for generating ultrasensitivity, elucidated cellular strategies for tuning the activation of the system, and highlighted regulatory principles that can be used in designing artificial signaling networks.

RESULTS

The Basic Synthetic Cascade

We constructed a basic synthetic cascade using the mammalian pathway of Raf-MEK-ERK (Figure 1A) in which the Raf level of the cascade is a hormone-binding domain fusion protein, eGFP: Δ Raf-1:ER-DD (Raf:ER), whose kinase activity is modulated by the addition of β -estradiol (McMahon, 2001). Consequently, the entire cascade is cytosolic (Figure S1 available online) and does not depend upon receptor-mediated membrane recruitment for activation. Single integrated copies of wild-type, epitope-tagged *Raf:ER*, *c-myc-MEK1* (MEK), and *His₆-ERK2* (ERK) were coexpressed from different auxotrophic loci by a reverse tTA-driven expression system (P_{tetO7}) (Bellí et al., 1998) induced with anhydrotetracycline (aTC). The system was stimulated with estradiol and assayed for steady-state activated ERK directly with quantitative western blotting (Figure 1B) to eliminate additional signal processing steps such as transcriptional activation (Mackeigan et al., 2005). As designed, our system is not bistable, as it does not fulfill the requirements of nonlinearity, feedback, and proper balance, and therefore the population mean reflects the unique activation state of the system. When the three kinases were expressed at equal concentration levels, the system reached a half-maximal response (EC_{50}) at 32 ± 1.4 nM and exhibited moderate ultrasensitivity (Figure 1C). The apparent Hill coefficient attained by this basic, constant-expression cascade, $n_H = 1.8 \pm 0.13$, fits well within the range of sensitivities observed in natural systems.

An ordinary differential equation (ODE) model of the basic cascade based on mass action kinetics (Huang and Ferrell, 1996) accurately captures the response (Figure 1C). All parameters and initial conditions were refined from literature values by globally fitting the Hill coefficient, signal strength, and EC_{50} to the experimental steady-state response curves of the basic and variable expression cascades (Extended Experimental Procedures). Parameter values were then held constant in simulating subsequent perturbations. The model assumes nonprocessive, dual-step phosphorylation events between sequential kinases, as has been demonstrated experimentally (Burack and Sturgill, 1997).

Insulation of this exogenous cascade from the host was assayed by a variety of methods. We identified possible interaction pathways by homology (Avruch, 2007) and previous findings in

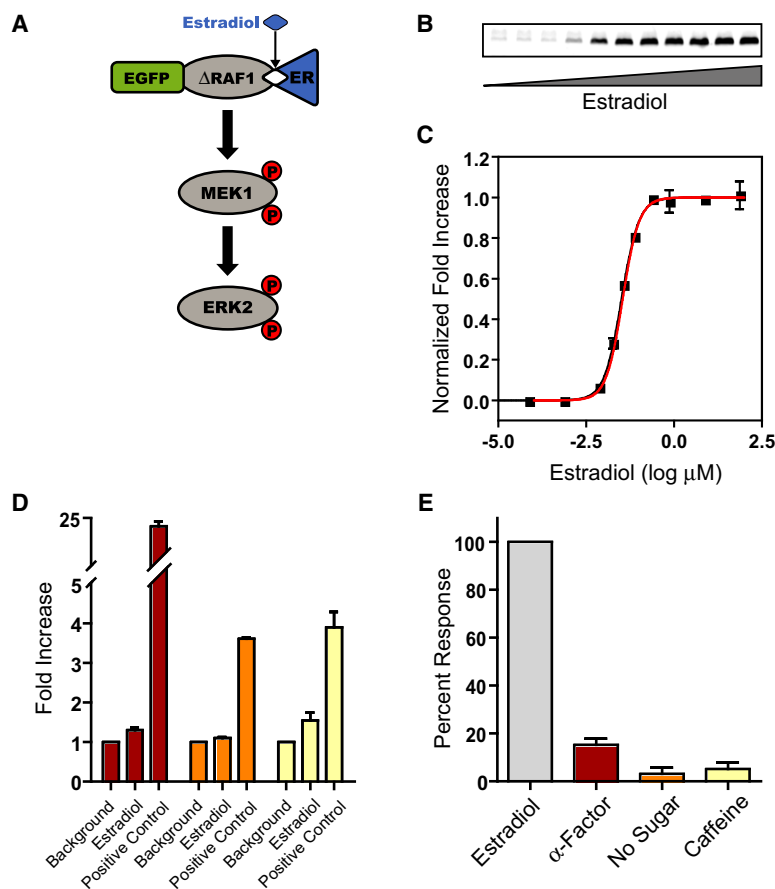


Figure 1. The Basic Synthetic Cascade

(A) Schematic of the basic synthetic cascade. *Raf:ER*, *MEK*, and *ERK* were coexpressed by P_{tetO7} . The kinase activity of *Raf:ER* is modulated by estradiol. See also Figure S1A.

(B) Representative western blot of steady-state ERK activation with increasing estradiol concentration.

(C) ERK activation in response to estradiol titration (black squares). The experimental data are the mean \pm SEM normalized to the fitted baselines. Data were fit with a modified Hill equation (black line). The model simulation results of the steady-state response profile for the basic cascade are shown as a red line. The system response is moderately ultrasensitive, with a Hill coefficient of 1.8 ± 0.13 and an EC_{50} of 32 ± 1.4 nM.

(D) Transcriptional activation of endogenous promoters by the basic synthetic cascade. The data are the mean \pm SEM *tdTomato* expression for the mating (red), invasive growth (orange), and cell wall integrity (yellow) pathways normalized to background.

(E) Activation of ERK by endogenous stimuli. Data are the mean \pm SEM phosphorylation level normalized to the estradiol stimulated cascade. See also Figure S1B.

the literature (Atienza et al., 2000) and consequently designed pathway-specific transcriptional reporters for the pheromone, invasive growth, and cell wall integrity pathways in *S. cerevisiae*. The synthetic cascade was stimulated with estradiol, and expression of *tdTomato* from each native pathway-specific promoter was determined by flow cytometry. We found minimal transcriptional activation from each of the endogenous pathways assayed when compared with pathway-specific positive controls (Figure 1D). In addition, we stimulated cells with agonists of endogenous MAPK pathways, including α factor (Bashor et al., 2008), glucose depletion (Cullen and Sprague, 2000), and caffeine (Jung et al., 2002), and determined the activation level of the synthetic MAPK cascade. We found almost no phosphorylation of ERK in response to glucose starvation and caffeine and $\sim 15\%$ activation in response to α factor despite the significant impact that these stimuli have on diverse cellular processes (Figure 1E). Further, we assayed for dephosphorylation of the synthetic cascade by endogenous phosphatases and found very modest interaction with these negative regulators (Figure S1). Taken together, these data indicate that the synthetic cascade is well insulated from the host, and the dynamic responses that we observe are a result of the minimal system itself and do not arise from unknown endogenous effectors.

The Variable Expression Cascades

In natural systems, *Raf*, *MEK*, and *ERK* are present at different concentrations, frequently increasing for sequential kinases. Further, the relative concentrations of cascade members vary significantly across different experimental systems (Ferrell, 1996). To understand the systems-level effects of this intrinsic perturbation, we constructed a cascade increasing the kinase concentration of each subsequent step, achieving ~ 10 -fold difference across the entire cascade (Figure 2A). Concentration was varied by expressing a single, integrated copy of *Raf:ER* with P_{tetO7} , high-copy *MEK* with P_{tetO7} , and high-copy *ERK* from the *Gal1* promoter (P_{Gal}) induced with galactose. The concentration range of this synthetic system was initially determined computationally by a global fit to the basic and variable cascades and was verified experimentally by quantitative ELISA against ERK (Figure S2). Under this perturbation, we found that the ultrasensitivity increased from $n_H = 1.8 \pm 0.13$ to 2.8 ± 0.19 , whereas the threshold was reduced from 32 ± 1.4 nM to 6.6 ± 0.14 nM (Figure 2B).

Qualitatively, this response is captured well by our computational model (Figure 2C). Interestingly, for this experimentally attainable range of parameter values, the model predicts that the *MEK* concentration will have a greater effect than that of *ERK* on both the ultrasensitivity and threshold of the response. We computationally varied *MEK* and *ERK* from 10 nM to 100 nM and determined the Hill coefficient and EC_{50} of each activation response (Figures 2D and 2E). The slope of the resulting surfaces is steeper when *MEK* is varied for a fixed value of *ERK* than when *ERK* is varied for a fixed *MEK* value. Therefore, we hypothesized that reducing the concentration of *MEK* in our variable cascade would increase the threshold and reduce the ultrasensitivity of the response.

To test this hypothesis, we built a variable expression cascade with a concentration of *MEK* in between those in the basic and

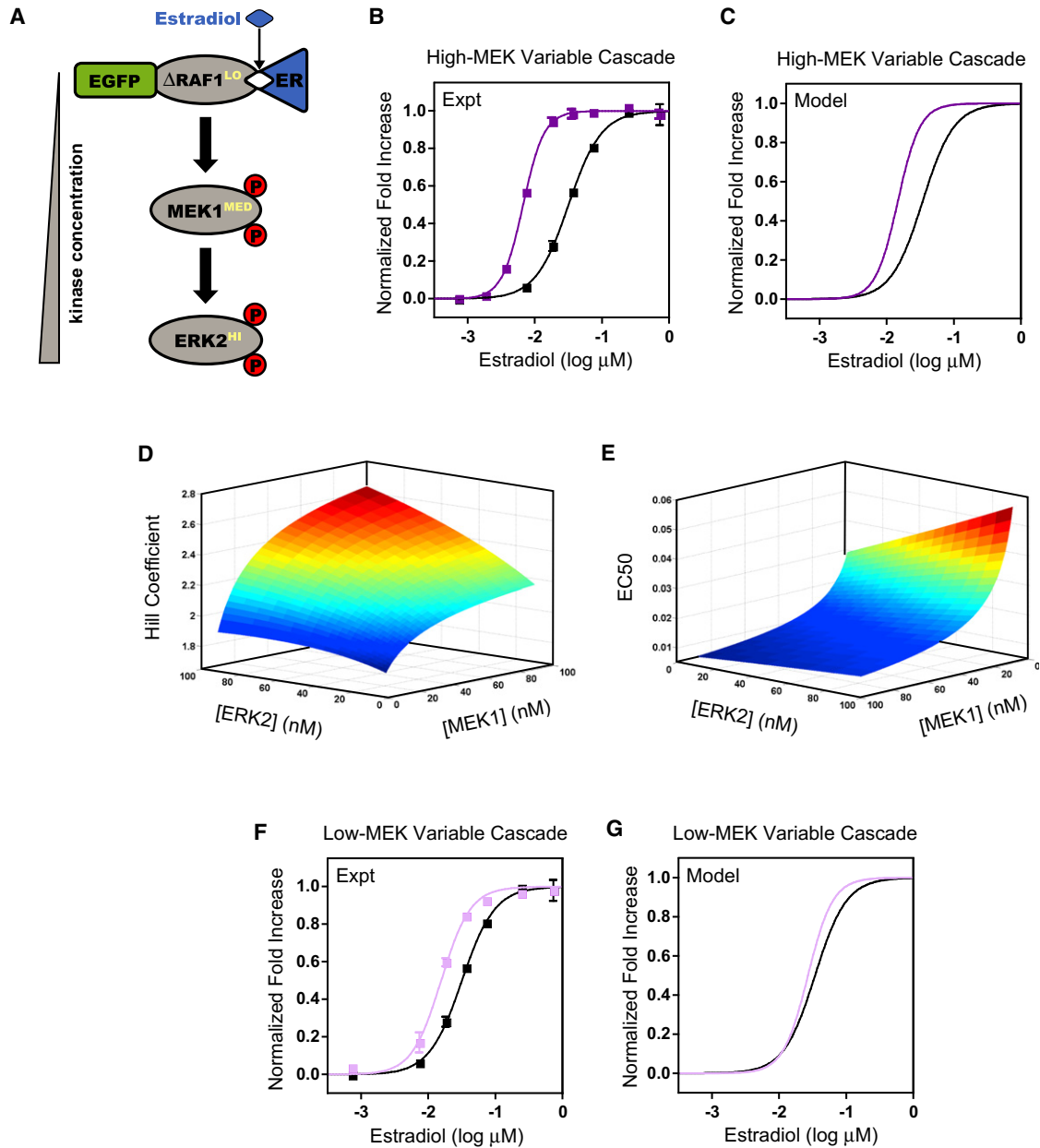


Figure 2. The Variable Expression Cascades

(A) Schematic of variable expression cascades. The kinase concentration increases at each tier in the cascade.

(B) Normalized fold increase of the high-MEK variable cascade (dark purple squares) and the basic cascade (black squares). The high-MEK variable cascade: single-copy *Raf:ER* expressed by P_{tetO7} , high-copy *MEK* expressed by P_{tetO7} , and high-copy *ERK* expressed by P_{Gal} (see also Figure S2). The data are the mean \pm SEM, normalized to the fitted baselines. Data were fit with a modified Hill equation (solid lines).

(C) Model simulations of the high-MEK variable cascade (dark purple) and the basic cascade (black). The fitted concentrations were *Raf:ER* = 10 nM, *MEK* = 80 nM, and *ERK* = 100 nM.

(D) Simulated Hill coefficient for the variable cascade in which both *MEK* and *ERK* were varied from 10 nM to 100 nM.

(E) Simulated EC_{50} for the variable cascade for the same parameters as in (D).

(F) Normalized fold increase of the low-MEK variable cascade (light purple squares) and the basic cascade (black squares). The low-MEK variable cascade: single-copy *Raf:ER* expressed by P_{tetO7} , single-copy *MEK* expressed by P_{Gal} , and high-copy *ERK* expressed by P_{Gal} . The data are the mean \pm SEM, normalized to the fitted baselines. Data were fit with a modified Hill equation (solid lines).

(G) Model simulations of the low-MEK variable cascade (light purple) and the basic cascade (black). The fitted concentrations were *Raf:ER* = 10 nM, *MEK* = 30 nM, and *ERK* = 100 nM.

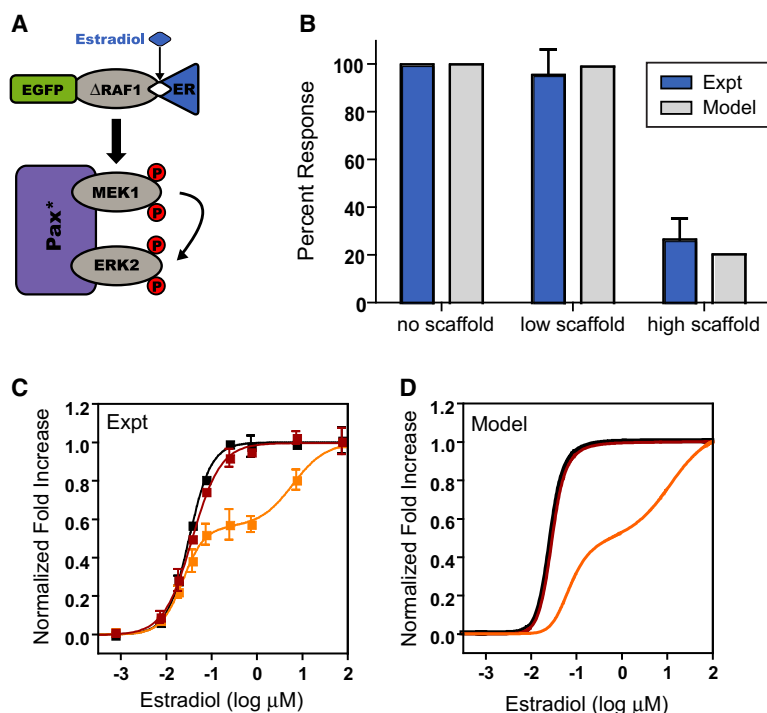


Figure 3. The Basic Cascade with Scaffolding

(A) Schematic of the basic cascade coexpressed with a two-member scaffold *pax**. See also Figure S3A.

(B) Percent response of the basic cascade alone and coexpressed with single-copy or high-copy *pax**. The experimental data (blue) are the mean \pm SEM, and the computational data (gray) are single values. All are normalized to the maximum activation of the basic cascade in the absence of scaffold.

(C) Normalized fold increase of the basic cascade (black squares) coexpressed with single-copy (red squares) or high-copy (orange squares) *pax**. The data are the mean \pm SEM, normalized to the fitted baselines (basic and single-copy *pax**) or the minimum and maximum values (high-copy *pax**) for each condition. The data were fit with a modified Hill equation (black and red lines) or biphasic dose-response equation (orange line).

(D) A compartmental model of no (black), low (red), or high (orange) scaffold expression. Simulations are normalized to the maximum value of each condition. See also Figure S3B.

original variable cascades (Figures 2F and 2G). In this low-MEK variable cascade, MEK was expressed from a single integrated copy by P_{Gal} , whereas the Raf:ER and ERK levels were kept the same in the two variable cascades. As predicted, lowering MEK expression resulted in both a reduction in ultrasensitivity from $n_H = 2.8 \pm 0.19$ to 2.0 ± 0.19 and an increase in threshold from $EC_{50} = 6.6 \pm 0.14$ nM to 15 ± 0.78 nM when compared with the high-MEK cascade (Figures 2B and 2F).

The Basic Cascade with Scaffolding

Scaffolding has been shown to be critical to signal transduction for some MAPK pathways (Elion, 2001), whereas, in others, the effects of colocalization remain unclear (Kolch, 2005). Furthermore, it is evident that scaffold concentration can be a strong determinant of MAPK activation (Burack and Shaw, 2000; Levchenko et al., 2000; Locasale et al., 2007). Therefore, we coexpressed the basic cascade with a modified two-member (MEK and ERK) scaffold, paxillin^{Y118D} (*pax**), and varied the scaffold concentration from ~ 30 nM to 100 nM by expression from single-copy and high-copy P_{Gal} (Figure 3A). Association of ERK and wild-type paxillin is regulated by phosphorylation of Tyr¹¹⁸ (Ishibe et al., 2003), which we mimicked with mutation to Asp and verified by coimmunoprecipitation (Figure S3). We found that moderate expression of *pax** from single-copy P_{Gal} results in a slight reduction in ultrasensitivity and a marginal effect on signal strength (Figure 3B). In contrast, we observed a marked decrease in signal strength to $\sim 25\%$ unscaffolded levels when *pax** is coexpressed from high-copy P_{Gal} . These results demonstrate that the Raf-MEK-ERK cascade is inherently catalytically efficient and does not depend on scaf-

folding to effectively propagate a signal. This is in contrast to some native yeast MAPK cascades, such as the mating and high-osmolarity pathways, that require scaffolding (Qi, 2005). Furthermore, our findings show that, when expressed near stoichiometric ratios that are optimal for signal propagation (Levchenko et al., 2000), scaffolding has a negligible effect on signal strength compared to that of the basic cascade.

In addition to a reduction in signal strength, we observed a two-phase dose-response in the presence of high scaffold concentrations (Figure 3C). Though paxillin is not homologous to native yeast MAPK scaffolds, exogenous paxillin has previously been shown to localize strongly to sites of polarized growth in yeast (Gao et al., 2004). Therefore, we hypothesized that this complex behavior arises from sequestration of the MAPK cascade, and we tested this hypothesis by explicitly including compartmentalization in our model of the basic cascade to generate a scaffold model. We found a single-phase ERK activation profile at moderate scaffold levels and a biphasic dose-response at high scaffold concentrations (Figure 3D). This multiphase response could not be generated with either a well-mixed model or a compartmental model in which paxillin cannot bind ERK (Figure S3), suggesting that sequestration of the cascade is necessary to elicit the observed response.

The Basic Cascade with Negative Regulation

In natural MAPK cascades, sequential activation by kinases is balanced by inactivation through negative regulation. Both theoretical (Heinrich et al., 2002) and experimental (Hornberg et al., 2005) work has demonstrated that activation and deactivation processes control distinct aspects of the MAPK response. Further, it has been shown that high concentrations of phosphatase can convert an ultrasensitive, bistable MAPK response into a proportional, transient activation profile via the disruption of positive feedback (Bhalla et al., 2002). We hypothesized that, even in the absence of feedback, the presence of negative regulators would tune the activation profile of the MAPK response.

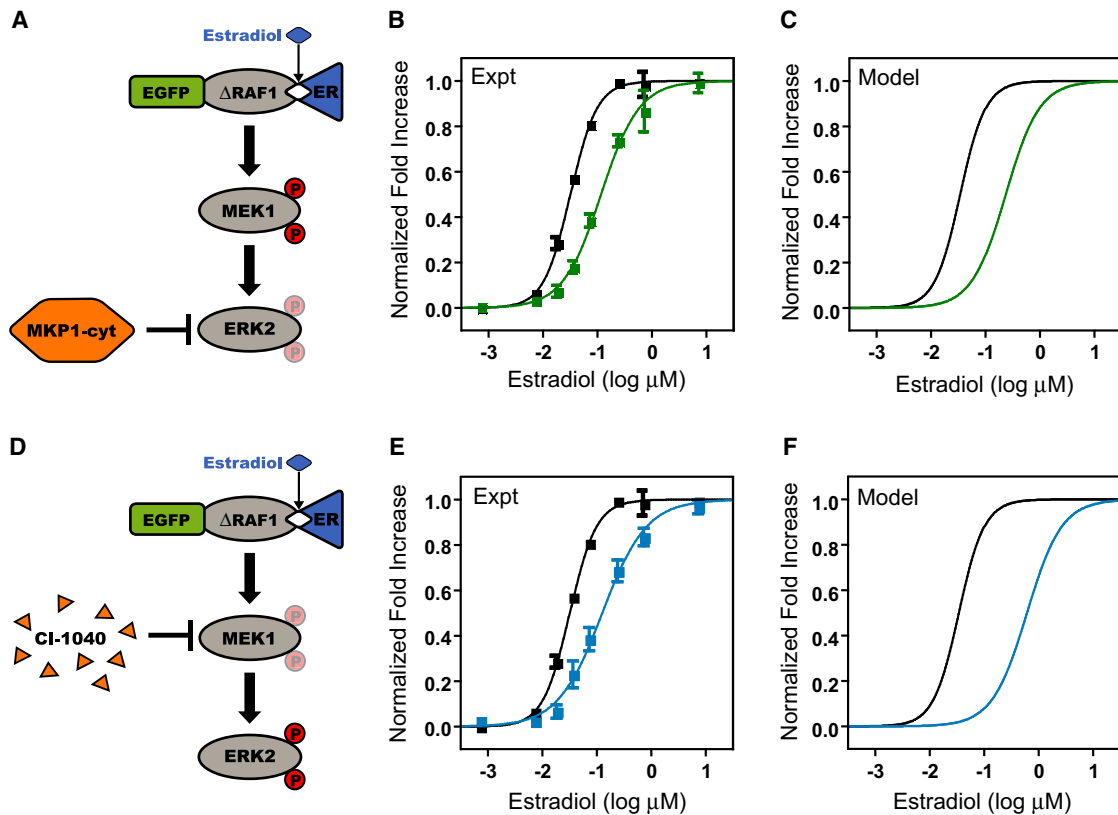


Figure 4. Negative Regulation of the Basic Cascade

(A) Schematic of the basic cascade coexpressed with the ERK phosphatase MKP1-cyt.

(B) Normalized fold increase of the basic cascade (black squares) coexpressed with high-copy MKP1-cyt (green squares) expressed by P_{Gal}. The data are the mean ± SEM, normalized to the fitted baselines. The data were fit with a modified Hill equation (solid lines).

(C) Model simulations with (green) and without (black) MKP1-cyt coexpression. Data are normalized to the maximum value of each condition.

(D) Schematic of the basic cascade with the MEK inhibitor CI-1040.

(E) Normalized fold increase of the basic cascade (black squares) pretreated with 50 nM CI-1040 for 30 min prior to estradiol stimulation (blue squares). The data are the mean ± SEM, normalized to the fitted baselines. The data were fit with a modified Hill equation (solid lines).

(F) Model simulations with (blue) and without (black) inhibitor pretreatment. Data are normalized to the maximum value of each condition.

We independently introduced two modes of negative regulation to a purely kinase-based cascade to test this hypothesis. First, we coexpressed the basic cascade with a weak, cytosolically targeted ERK phosphatase, MKP-1^{L16A/L17A} (MKP1-cyt) (Wu et al., 2005), from single-copy P_{Gal} (Figure 4A). The presence of this dual-specificity phosphatase affected not only the threshold of the system, which increased from 32 ± 1.4 nM to 110 ± 9.3 nM, but also the ultrasensitivity, which was reduced from $n_H = 1.8 \pm 0.13$ to 1.2 ± 0.11 (Figure 4B). A model of the basic cascade with this additional enzymatic reaction predicted both of these features qualitatively (Figure 4C).

In addition to enzymatic negative regulation of ERK, we perturbed the system with the small molecule MEK inhibitor, CI-1040 (Figure 4D). CI-1040 is a strong noncompetitive but reversible binder that targets the unphosphorylated form of MEK and renders the kinase catalytically inactive (Ohren et al., 2004). We found similar results to coexpression of MKP1-cyt in that the Hill coefficient decreased from 1.8 ± 0.13 to 1.1 ± 0.12 in the presence of 50 nM CI-1040, and the threshold increased from 32 ± 1.4 nM to 120 ± 10 nM (Figure 4E). A model of the basic

cascade with an additional inhibitor-binding reaction captured both features of this response (Figure 4F). Whereas these results are similar to those observed under ERK phosphatase coexpression, the mechanisms behind enzymatic and binding-mediated regulation are different. CI-1040 effectively lowers the concentration of available MEK, thereby reducing the ultrasensitivity and increasing the threshold. The converse effect is seen in the variable cascade, in which increasing MEK concentration results in greater steepness and a lower response threshold.

Integrating Variable Expression Cascades with Negative Regulation

Our computational model captures all of the qualitative trends seen in the experimental data for individual perturbations to the basic synthetic cascade. We therefore used the model to probe the effects of combining different perturbations over a broader range of parameters. Initially, we explored the intrinsic perturbation of concentration variation within the basic cascade (Figure 5A), as MEK and ERK were varied from 10 nM to 2 μM and 10 nM to 10 μM, respectively, and the Hill coefficient, EC₅₀, and

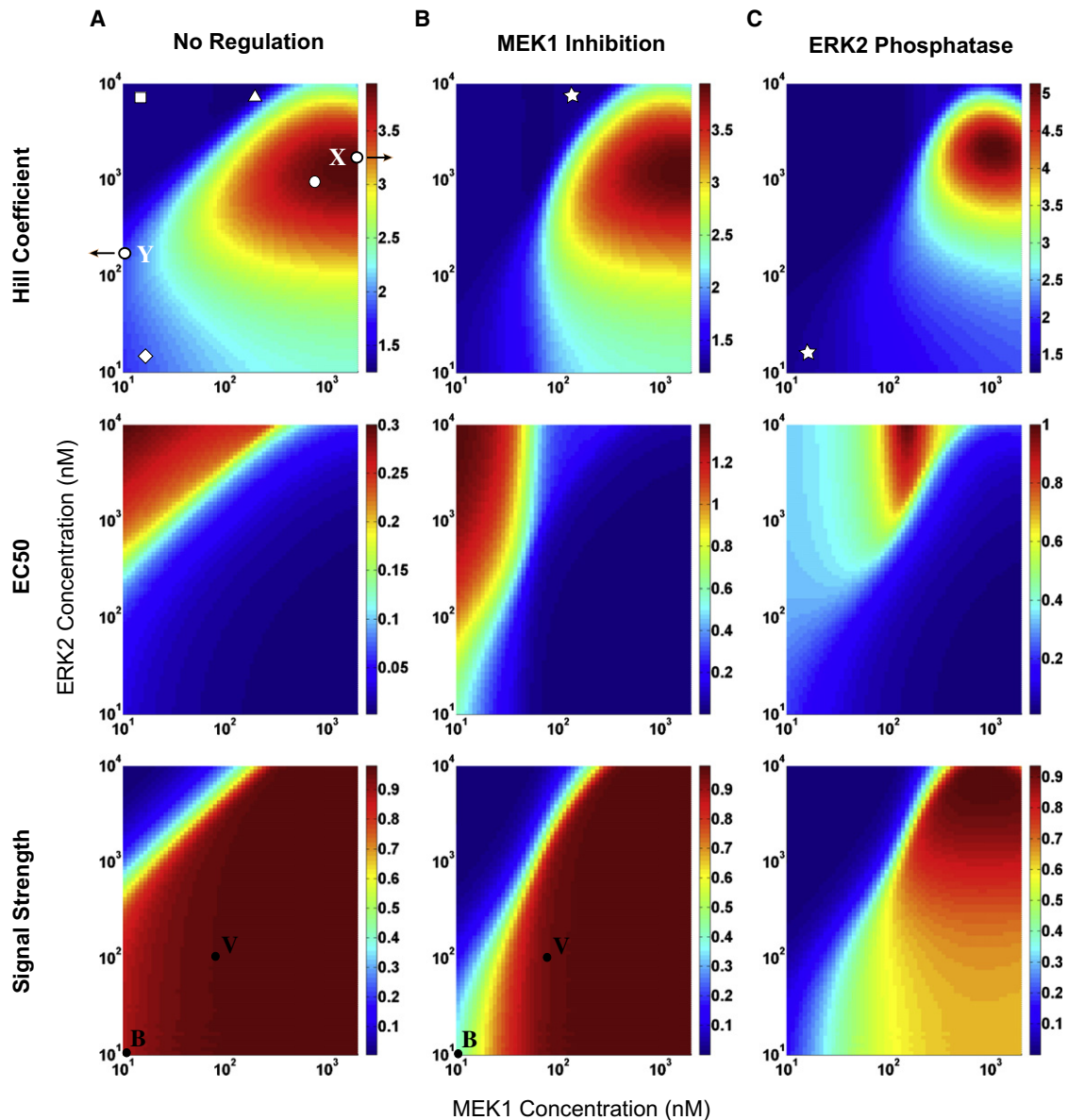


Figure 5. Computational Analysis of Concentration Variation and Negative Regulation

(A) No regulation: Raf:ER was held constant at 10 nM, and MEK and ERK were varied from 10 nM to 2 μ M and 10 nM to 10 μ M, respectively. The top panel shows the Hill coefficient, the middle panel shows the EC_{50} , and the bottom panel shows the normalized signal strength. (Top) The point marked “X” indicates the *Xenopus* cascade, and the point marked “Y” indicates the yeast pheromone cascade. Each symbol represents a distinct class of system response (Table S1). For example, the square identifies systems for which the Hill coefficient is low, the EC_{50} is high, and the normalized signal strength is low. (Bottom) The point marked “B” denotes the basic cascade, and the point marked “V” denotes the high-MEK variable cascade. See also Figure S4 and Figure S5.

(B) MEK inhibition: The same parameter space as in (A) modeled with 50 nM Cl-1040. (Top) The star represents a distinct system response not seen in the absence of negative regulation. (Bottom) “B” indicates the basic cascade, and “V” indicates the high-MEK variable cascade.

(C) ERK phosphatase: The same parameter space as in (A) modeled with 100 nM MKP1-cyt coexpression. The star represents the system response in (B) achieved in a different region of parameter space.

signal strength were determined over the entire parameter space. Strikingly, the Hill coefficient is strongly biphasic, whereas the EC_{50} and signal strength are monotonic. This enables the decoupling of ultrasensitivity from other signal characteristics simply by adjusting the relative concentrations of cascade members. For example, at high MEK concentrations,

the EC_{50} is low and the signal strength is high, whereas the Hill coefficient can be independently tuned from ~ 2 to 4 by varying the ERK concentration. Conversely, at low MEK levels, the Hill coefficient is low for all ERK concentrations, whereas the EC_{50} and signal strength vary considerably as a function of ERK level. The decoupling of signal characteristics in the absence of

extrinsic perturbation highlights the inherent flexibility in a three-tiered kinase cascade.

We then applied the extrinsic perturbation of MEK inhibition (Figure 5B) and found that the Hill coefficient is also biphasic with ERK, yet the transitions become steeper with respect to MEK concentration. The threshold is shifted so that, for low MEK, the EC_{50} is high for a larger range of ERK concentration than in the unregulated case. Not surprisingly, the region of maximal signal strength is smaller, showing a marked reduction in gain for low MEK and low ERK concentrations. We show in Figure 4 that two modes of inhibition were similar for given parameter values; however, modeling negative regulation with ERK phosphatase reveals very different behavior from binding inhibition of MEK when surveyed over a wider parameter space (Figure 5C). Though experimentally we see a decrease in ultrasensitivity upon phosphatase coexpression (Figures 4B and 4C), our model predicts that, in a different region of parameter space, the Hill coefficient will be greater than that of the basic cascade alone. Furthermore, in the presence of phosphatase, the EC_{50} becomes biphasic, and the signal strength exhibits a broad range of intermediate values. These nonmonotonic profiles increase the possible combinations of signal characteristics and further enable the decoupling of signal aspects.

Theoretical Analysis of Cascade-Generated Ultrasensitivity

Several mechanisms leading to MAPK ultrasensitivity have been posited including zeroth-order ultrasensitivity (Goldbeter and Koshland, 1981), dual-step phosphorylation, and competitive inhibition (Ferrell, 1996). Our synthetic cascade is not subject to either zeroth-order ultrasensitivity or competitive inhibition, but it is affected by dual-step phosphorylation of MEK and ERK. Interestingly, our experimental and computational results both indicate that kinase concentration itself, even in the absence of zeroth-order effects, contributes to MAPK ultrasensitivity (Figure 2 and Figure 5). Therefore, we simulated dual-step and single-step mass action kinetic models over a wide range of concentrations to dissect the contributions of multistep processes and relative kinase concentration to the overall ultrasensitivity of ERK activation (Figure 6A). In addition, we generated a Hill equation that matched the dose-response of active MEK from these explicit models and used this aggregate equation as the stimulus to a final, explicit ERK step. The relative kinase concentrations chosen correspond to distinct sets of behaviors identified in Figure S4 and Figure S5.

We found that, in all cases, the ultrasensitivity arising from explicit cascading is greater than simple multiplicative accumulation (Figure 6B). Furthermore, when each level in the cascade is modeled as a single phosphorylation process (i.e., when dual-step phosphorylation is eliminated), the supermultiplicative generation of ultrasensitivity by cascading is maintained and is strongly influenced by concentration, though the overall ultrasensitivity is considerably lower than that of dual-step cascades. To explore the mechanisms underlying this generation of ultrasensitivity by cascading, we analyzed the dose-response curves of each species accounted for by mass action kinetics (Table S2). When the cascade is modeled explicitly, active MEK exists in either a free or complex-bound state, and the behavior of

these distinct species varies dramatically depending on the relative enzyme and substrate concentrations. For example, when the ultrasensitivity of ERK is high, this steepness arises specifically from the complex-bound MEK species even though the total MEK ultrasensitivity is low (Figure 6C). In contrast, when the ERK ultrasensitivity is low, there is a negligible difference between the dose-responses of each MEK species, as all have low ultrasensitivity. Notably, this phenomenon occurs for both dual-step and single-step kinase activation. Furthermore, when the Raf and MEK levels of the cascade are aggregated into a single Hill equation that accurately mimics the dose-response of total active MEK in the explicit model, the complex-bound MEK species has a lower ultrasensitivity than in the explicit model alone (Figure 6D). Therefore, the multitiered structure of MAPK cascades does not simply serve to accumulate ultrasensitivity multiplicatively, but it can actually generate ultrasensitivity *de novo* in a concentration-dependent manner through a distribution of intermediate species. An explicit model that accounts for all physiologically relevant species, without simplifying assumptions (i.e., Hill equation and Michaelis-Menten approximations) or the inclusion of phosphatases, captures this mechanism of ultrasensitivity.

MEK Inhibition of the Variable Cascade

Based on our computational model, we predicted that applying 50 nM CI-1040 to the high-MEK variable cascade would decrease the ultrasensitivity, increase the threshold, and leave the signal strength unaffected. This is in contrast to the basic cascade in which the signal strength is predicted to be significantly lower upon MEK inhibition. As shown in Figure 5, both the basic and variable cascades are in the high signal strength region in the absence of MEK inhibition, yet with inhibition, they are separated by a sharp transition from low to high signal strength. In this parameter regime, the Hill coefficient and EC_{50} become decoupled from the signal strength of the system. Therefore, we tested MEK inhibition in the variable cascade and observed a reduction in ultrasensitivity from $n_H = 2.8 \pm 0.19$ to 1.7 ± 0.17 and an increase in EC_{50} from 6.6 ± 0.14 nM to 16 ± 1.1 nM (Figure 7A) as predicted by the model (Figure 7B). Strikingly, the basic cascade shows a significant reduction in signal strength, to ~25% uninhibited levels (Figures 7C and 7D), whereas the response of the variable cascade is unaffected by MEK1 inhibition (Figures 7E and 7F). These computational and experimental results demonstrate both the ability to decouple signal characteristics and the great degree of plasticity exhibited by the MAPK topology itself through the use of multiple relatively simple perturbations.

DISCUSSION

In this study, we used a synthetic biology approach to explore factors regulating the systems-level properties of a minimal MAPK module. Synthetic biology is a rapidly evolving discipline that has both engineered novel biological functions and contributed to the current understanding of natural processes (Grunberg et al., 2010; Hasty et al., 2002; Khalil and Collins, 2010; Kiel et al., 2010; Sprinzak and Elowitz, 2005). By reconstructing a biological system, applying perturbations, and measuring the

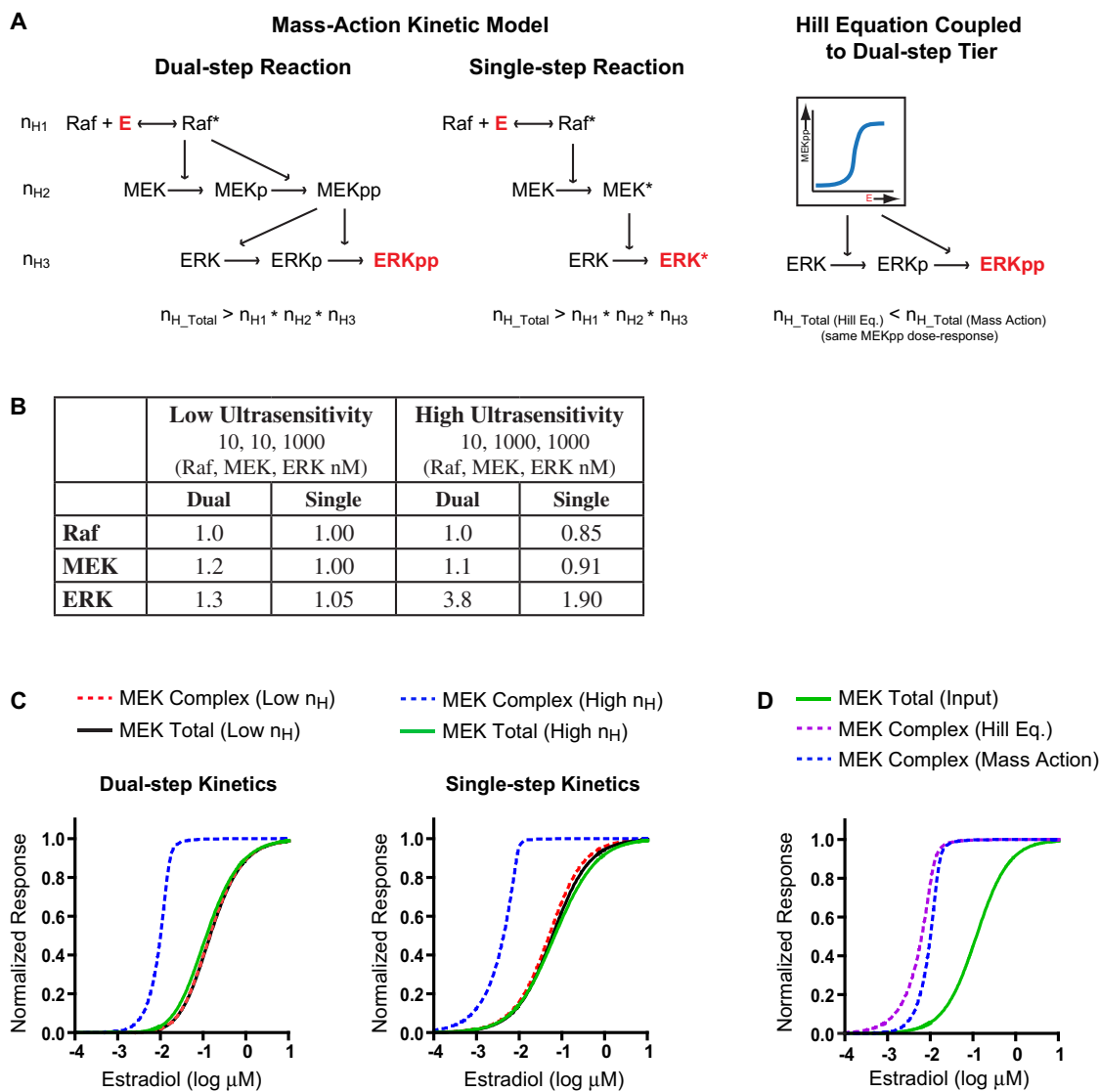


Figure 6. Theoretical Analysis of Cascade-Generated Ultrasensitivity

(A) Schematic of dual-step and single-step mass action kinetic models and a lumped Hill equation model coupled to a dual-step tier.

(B) The Hill coefficients of each level of the cascade for both dual- and single-step mass action kinetic models for representative low- and high-ultrasensitivity systems. See also Table S2.

(C) Simulations of distinct active MEK species for dual- and single-step cascades at the relative concentrations indicated in (B).

(D) Comparison of simulated active MEK complex species with the Hill equation and mass action kinetic models for the same input function (total active MEK) in the high-ultrasensitivity system.

response, we can test and expand our understanding of how the system works and gain insight into how to modify it. Well-defined synthetic systems obviate some of the difficulties of natural systems that have an inherent degree of uncertainty with respect to molecules and topology. We used yeast as an *ex vivo* system to build a purely exogenous protein interaction network based on the mammalian ERK1/2 pathway. We also used mechanistic computational modeling to directly demonstrate conceptually new behaviors, such as cascade-based generation and concentration-based tuning of ultrasensitivity, independent of any experimental system.

Our simple synthetic cascade was used to investigate the role of scaffolding in shaping the activation profile of ERK. In contrast to the prozone effect, we see a monotonic dependence on scaffold concentration in which the signal strength is strong when the scaffold is either absent or expressed at optimal stoichiometric ratios and greatly attenuated at high scaffold concentrations. Our data show that the synthetic cascade is catalytically efficient, and therefore this monotonic response occurs because the cascade is not aided by the presence of scaffold. The disruption of signal strength seen at high scaffold concentrations can arise through multiple mechanisms,

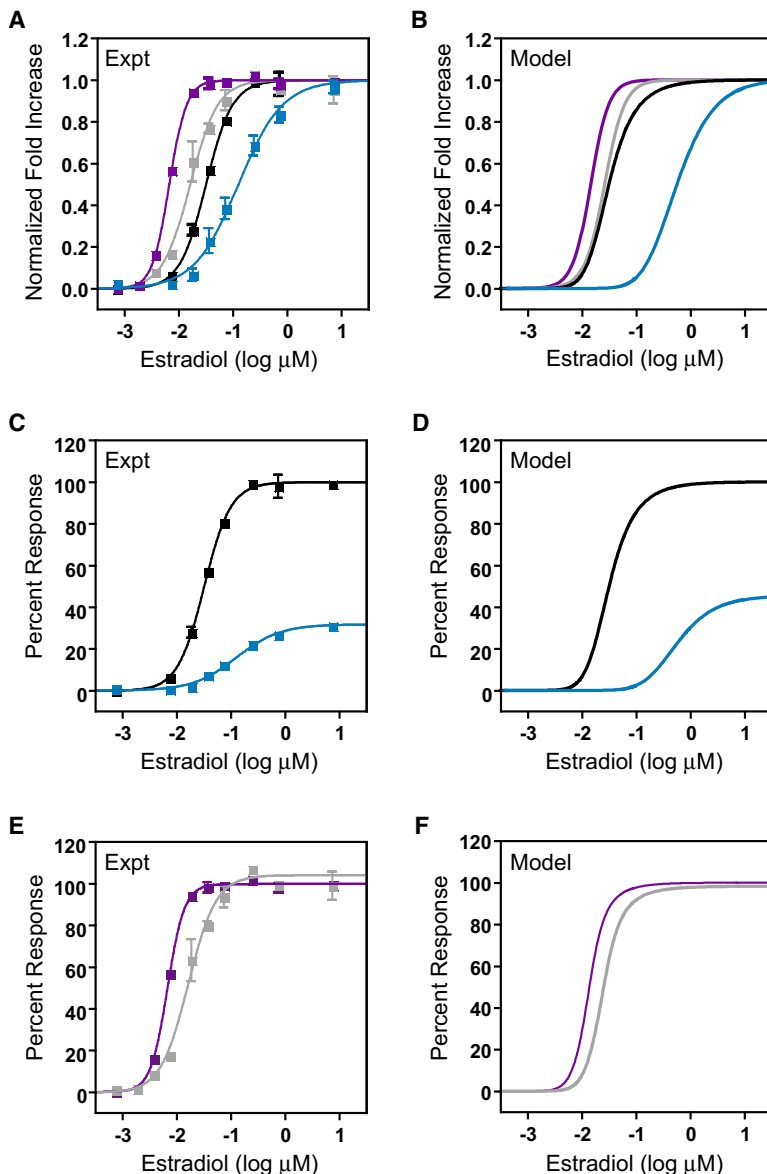


Figure 7. MEK Inhibition of the Variable Cascade

(A) Normalized fold increase for the high-MEK variable cascade with (gray squares) and without (dark purple squares) pretreatment with 50 nM CI-1040 and for the basic cascade with (blue squares) and without (black squares) this inhibitor. The data are the mean \pm SEM normalized to the fitted base-lines for each condition. The data were fit with a modified Hill equation (solid lines).

(B) Model simulations of the experimental conditions described in (A).

(C) Percent response of the basic cascade with (blue squares) and without (black squares) 50 nM CI-1040 pretreatment. The data are the mean \pm SEM normalized to the maximum activation of the basic cascade in the absence of inhibitor.

(D) Model simulations of the experimental conditions described in (C).

(E) Percent response of the high-MEK variable cascade with (gray squares) and without (dark purple squares) 50 nM CI-1040 pretreatment. The data are the mean \pm SEM normalized to the maximum activation of the high-MEK variable cascade in the absence of inhibitor.

(F) Model simulations of the experimental conditions described in (E).

including combinatorial inhibition or dampened amplification. Combinatorial inhibition occurs when individual kinases become sequestered on separate scaffold molecules, as has been posited experimentally for the KSR1 and JIP1/2 scaffolds (Burack and Shaw, 2000) and computationally for a generic two-member scaffold (Levchenko et al., 2000). More recent theoretical work on the MAPK cascade found that scaffolds lower the amplification and magnitude of a signal under conditions conducive to signal transduction in the absence of scaffold (Locasale et al., 2007). This effect was mediated entirely by dampening of amplification through the cascade and did not involve combinatorial inhibition.

We demonstrated that varying the relative concentrations of proteins intrinsic to the three-tiered MAPK module enables great flexibility of the system response and that key signal character-

istics can be decoupled under certain parameter regimes (Figure 5 and Figure 7). This suggests a potential cellular strategy for tuning the response of the MAPK cascade in distinct biological contexts without changing the module topology itself. Controlling protein expression levels through either gene expression or posttranslational modification presents an effective and robust method for varying the activation profile of MAP kinases. Ground-breaking work on ultrasensitivity in the *Xenopus* oocyte Mos-MEK-p42 MAPK cascade revealed a sharply switch-like, irreversible response (Xiong and Ferrell, 2003). Interestingly, the relative concentrations of these proteins (Mos, 3 nM; MEK, 1200 nM; p42 MAPK, 330 nM) (Ferrell, 1996) map the system to the high-ultrasensitivity region of our theoretical heat map (Figure 5, marked X). In contrast, the Ste11-Ste7-Fus3 MAPK cascade of the pheromone pathway in yeast

has been shown to exhibit a less ultrasensitive activation profile (Hao et al., 2008; Poritz et al., 2001). Strikingly, the relative concentrations of these proteins (Ste11, 41 nM; Ste7, 37 nM; Fus3, 470 nM) (Ghaemmghami et al., 2003) place this cascade in the low-ultrasensitivity region of our theoretical framework (Figure 5, marked Y). Though it is clear that factors extrinsic to the module, such as positive feedback, scaffolding, and subcellular compartmentalization, play important roles in determining the activation profile of these natural signaling cascades, these systems may be primed for their respective behaviors through the intrinsic parameter of kinase concentration.

We also identified kinase cascading as a mechanism for de novo generation of ultrasensitivity, and we showed that this effect is strongly concentration dependent, though it is not mediated by zeroth-order ultrasensitivity or solely by dual-step

phosphorylation. We used a mass action kinetic model, based largely on the seminal work of Huang and Ferrell (1996), to explore the role of cascading in generating ultrasensitivity. The model presented in their work specifically accounted for dual-step dephosphorylation at each level of the cascade and was therefore subject to heightened ultrasensitivity through an additional dual-step process and through zeroth-order ultrasensitivity by creation of an activation-deactivation cycle. We systematically deconstructed this model, first removing phosphatases and then simulating activation of each kinase as a single-step reaction; by eliminating these additional sources of ultrasensitivity, we were able to analyze the inherent contributions of the kinase-cascading architecture in generating MAPK ultrasensitivity. We found that, over a broad range of relative kinase concentrations, the steepness of each subsequent tier increases in a greater than multiplicative manner. This result was surprising, given that previous theoretical studies (Brown et al., 1997; Ferrell, 1997) suggest that the ultrasensitivity of sequential levels in a cascade accumulates in a multiplicative or submultiplicative manner. In contrast, our analysis shows that, instead of simply passing steepness from one level to the next, cascading can lead to an output response whose Hill coefficient is greater than the product of the coefficients of the previous levels (Figure 6). The difference between our analysis and previous work arises because earlier models relied essentially on independent, though sequential, Hill equations in which there is one output species for a given input stimulus concentration. In our analysis, each level of the cascade contains a distribution of species (i.e., different phosphorylation and complexation states), and the concentrations of these species depend on both the kinetic parameters of each reaction and the total concentrations of Raf, MEK, and ERK. For a given input stimulus, this explicit apportioning of species results in a different output than the corresponding Hill equation approximation (Figure 6D), even at steady state, and the behaviors of these distinct species vary considerably as a function of concentration (Figure 6C).

Furthermore, a biphasic Hill coefficient is a prominent feature of concentration variation seen under all conditions (Figure 5). Ultrasensitivity is low when either MEK or ERK is limited, and the extent of limitation for a given set of concentrations can be determined by the specific MEK species generated (Figure S4 and Figure S5). The optimum Hill coefficient will depend not only on the molarity of the individual kinases, but on parameters of activation as well. Previous work has shown that introducing compensatory alterations in the association and dissociation rate constants of Ras-Raf binding has a significant impact on the activation profile of ERK (Kiel and Serrano, 2009). Moreover, the influence of these different parameters is cell type specific, indicating that the plasticity of MAPK signaling is multifaceted.

The steepness and magnitude of the biphasic Hill coefficient become enhanced through the addition of a phosphatase (Figure 5C) because of the introduction of an activation/deactivation cycle. The mechanism of dephosphorylation is also nonprocessive (Zhao and Zhang, 2001) and can contribute to the ultrasensitivity of the response. In addition, the generation of a cycle may further increase ultrasensitivity through zeroth-order effects in this region of parameter space. Interestingly, the addition of a cycle also results in a biphasic profile for the EC_{50} that is

in contrast to MEK inhibition, in which no enzymatic cycle is created. Under MEK inhibition, the response is similar to that of the unregulated system, but the region boundaries become shifted, creating further opportunities to independently tune certain signal characteristics. We demonstrate experimentally that the signal strength of the system can be decoupled from the EC_{50} and Hill coefficient (Figure 7) and identify additional possibilities for isolating distinct signal features through this theoretical analysis.

Looking across each signal characteristic for different modes of regulation (Figure 5), it becomes apparent that some combinations of features are possible, whereas others do not arise (Table S1). We find that, for a low Hill coefficient, any combination of other signal aspects is attainable. However, to achieve a steep ultrasensitivity, the cascade must signal efficiently, which requires that the EC_{50} be low and the signal strength be high. To build a MAPK cascade with a sharply switch-like response and a high threshold, additional modes of regulation must be employed. From a synthetic biology perspective, this type of analysis is useful in designing novel signaling cascades. For example, several research groups have successfully engineered endogenous receptors with altered specificity (Dwyer et al., 2003; Looger et al., 2003) or expressed exogenous receptors (Chen and Weiss, 2005) that recognize novel ligands and relay the signal through endogenous pathways. We have identified mechanisms for tuning the threshold and ultrasensitivity of a ubiquitous relay module, and therefore these principles may be useful in altering biosensor sensitivity, building kinase-based logic gates, or tuning native signaling responses (such as differentiation, survival, or apoptosis) in engineering cells and tissues. Synthetic biology at the level of posttranslational modification is currently at the cusp of rapid discovery and growth (Grunberg et al., 2010; Kiel et al., 2010). In this study, we have shown how the key signal characteristics of strength, threshold, and ultrasensitivity in a ubiquitous and essential signaling module can be controlled through simple and accessible perturbations.

EXPERIMENTAL PROCEDURES

Plasmid and Strain Construction

Complete tables of plasmids and strains used in this study can be found in Table S3 and Table S4, respectively. All plasmid construction was done using standard cloning methods for PCR amplification, restriction digest, ligation, and bacterial transformation. Integration vectors were derived from pRS403-6, and episomal vectors were derived from pESC-leu and pESC-ura (all from Stratagene). The anhydrotetracycline-regulated tetO₇ promoter and reverse tTA cDNA were cloned from pCM252 (EuroScarf). *MKP-1^{LT6A/L17A}* cDNA was obtained from Anton Bennett through Addgene plasmid 13478. Additional cDNAs were kindly provided by the following: *His₆-ERK* and *c-myc-MEK* from Natalie Ahn, *eGFP:ΔRaf-1:ER-DD* from Steen Hansen, *c-myc-paxillin* from Lloyd Cantley, the pTy1 promoter from Gerald Fink, and the *YIL117c* promoter from David Levin. *Paxillin^{Y118D}* was generated by site-directed mutagenesis with standard PCR techniques and sequence verified. Yeast transformation was done with the LiAc method in selective synthetic complete dropout media. Single integration was confirmed by PCR screening of genomic DNA.

Growth and Induction

All strains were grown from a fresh colony in synthetic complete (SC) dropout media (0.67% yeast nitrogen base without amino acids, 2% glucose, 0.14% His-Leu-Trp-Ura dropout mix supplemented with appropriate amino acids) for 24 hr. Cells were grown with shaking at 30°C. Liquid culture was diluted

into SC media with 2% galactose (no glucose) and 0.5 $\mu\text{g/ml}$ aTC (Sigma Aldrich) and grown for 16 hr. One sample per estradiol titration was grown without aTC to determine the background. Cells were stimulated with β -estradiol (Sigma Aldrich) for 45 min for basic cascades and 120 min for variable cascades. For inhibitor experiments, cells were pretreated for 30 min with Cl-1040 (Axon Medchem) prior to estradiol stimulation. One milliliter cultures ($\text{OD}_{660} = 0.7\text{--}0.8$) were lysed for analysis by incubating them in 1 ml fresh 0.1 M NaOH at room temperature for 5 min. They were then resuspended in 50 μl lysis buffer (120 mM Tris-HCl [pH 6.8], 10% glycerol, 4% SDS, 5% β -mercaptoethanol, and 0.004% bromophenol blue), incubated at 95°C for 3 min, and frozen at -20°C . Estradiol titration was done in triplicate for each strain.

Quantitative Western Blotting and Analysis

Standard SDS-PAGE electrophoresis and transfer procedures were used. Primary antibodies used include anti-phospho-p44/42 MAP kinase (Cell Signaling Technology), anti-ERK (BD Biosciences), anti- α -tubulin (AbD Serotech), and anti-MEK (BD Biosciences). Secondary antibodies used with the Odyssey Infrared Imaging System (Li-Cor Biosystems) include goat- α -mouse-IRDye700DX (Rockland), goat- α -rabbit-IRDye800CW (Rockland), and donkey- α -rat-IRDye800CW (Rockland). Standard western blotting procedures were used with Odyssey blocking buffer (Li-Cor). Phospho-ERK intensity was normalized by OD_{660} and total ERK signal or α -tubulin as loading controls.

Each individual experiment was log transformed and fit to a modified Hill equation (1) with a nonlinear least-squares method using Prism 4 software (GraphPad Software) and then normalized to the fitted baselines (R_o and R_{max}):

$$R = R_o + \frac{(R_{max} - R_o) * L^{n_H}}{L^{n_H} + EC_{50}^{n_H}} = R_o + \frac{(R_{max} - R_o)}{1 + (10^{(\log EC_{50} - \log L)^{n_H}})} \quad (1)$$

The left-hand equality is the standard Hill equation with lower and upper baselines R_o and R_{max} , respectively; R is the system response (signal strength), L is the ligand concentration, n_H is the Hill coefficient, and EC_{50} is the half-maximal concentration of activation (threshold). The right-hand equality is a rearrangement of the Hill equation that was used to fit log-transformed data. The normalized data for each strain were pooled, and the mean and standard error of the mean were calculated with Prism 4.

Transcriptional Activation of Endogenous Pathways

The minimal promoter of *Fus1* (-266 to $+1$) fused to *tdTomato* was custom synthesized by Geneart with NotI and BamHI sites flanking the promoter region. Additional promoters, a modified Ty1 promoter amplified from BMH261 (Madhani and Fink, 1997) and the *Y1L117c* promoter excised directly from p1366 (Jung et al., 2002), were subcloned into NotI and BamHI. Transformed strains were grown as above and stimulated with either β -estradiol for 2 hr or positive controls: 2.5 μM α factor for 2 hr (pheromone and cell wall integrity), glucose starvation for 4 hr (invasive growth), and 40 mM caffeine for 6 hr (cell wall integrity). *tdTomato* expression was quantified by flow cytometry using a Guava flow cytometer (Millipore).

Model Formulation

We used an ordinary differential equation (ODE)-based, deterministic approach to model the basic cascade and its variations. In the basic cascade, protein synthesis, binding reactions, dual-step phosphorylation, and protein degradation reactions were explicitly included. All binding and activation reactions were modeled with mass action kinetics and did not rely on approximations of rapid equilibrium or pseudosteady state (Michaelis-Menten). The series of ODEs for each model was solved using the numerical stiff solver ode23s in MATLAB (The Mathworks). Steady-state response plots, as well as 3D surface and 2D phase plots, were generated in MATLAB. Further descriptions of the various model formulations are given in the Extended Experimental Procedures, and model definitions, reactions, equations, parameters, and initial conditions are given in Table S5, Table S6, Table S7, Table S8, and Table S9, respectively.

SUPPLEMENTAL INFORMATION

Supplemental Information includes Extended Experimental Procedures, five figures, and nine tables and can be found with this article online at doi:10.1016/j.cell.2010.12.014.

ACKNOWLEDGMENTS

This work was supported by the National Institutes of Health (NIH) through the NIH Director's Pioneer Award Program, grant number DP1 OD00364, and by the Ellison Medical Foundation and the Howard Hughes Medical Institute (to J.J.C.); and by the American Heart Association, grant number 0835132N, and startup funds from the University of Pennsylvania (to C.A.S.). We also thank Natalie Ahn, Lloyd Cantley, Gerald Fink, Steen Hansen, and David Levin for kindly providing cDNA.

Received: September 1, 2009

Revised: October 1, 2010

Accepted: December 10, 2010

Published: January 6, 2011

REFERENCES

- Atienza, J.M., Suh, M., Xenarios, I., Landgraf, R., and Colicelli, J. (2000). Human ERK1 induces filamentous growth and cell wall remodeling pathways in *Saccharomyces cerevisiae*. *J. Biol. Chem.* 275, 20638–20646.
- Avruch, J. (2007). MAP kinase pathways: the first twenty years. *Biochim. Biophys. Acta* 1773, 1150–1160.
- Bagowski, C.P., Besser, J., Frey, C.R., and Ferrell, J.E., Jr. (2003). The JNK cascade as a biochemical switch in mammalian cells: ultrasensitive and all-or-none responses. *Curr. Biol.* 13, 315–320.
- Bashor, C.J., Helman, N.C., Yan, S., and Lim, W.A. (2008). Using engineered scaffold interactions to reshape MAP kinase pathway signaling dynamics. *Science* 319, 1539–1543.
- Bellí, G., Garí, E., Piedrafita, L., Aldea, M., and Herrero, E. (1998). An activator/repressor dual system allows tight tetracycline-regulated gene expression in budding yeast. *Nucleic Acids Res.* 26, 942–947.
- Bhalla, U.S., Ram, P.T., and Iyengar, R. (2002). MAP kinase phosphatase as a locus of flexibility in a mitogen-activated protein kinase signaling network. *Science* 297, 1018–1023.
- Brown, G.C., Hoek, J.B., and Kholodenko, B.N. (1997). Why do protein kinase cascades have more than one level? *Trends Biochem. Sci.* 22, 288.
- Burack, W.R., and Sturgill, T.W. (1997). The activating dual phosphorylation of MAPK by MEK is nonprocessive. *Biochemistry* 36, 5929–5933.
- Burack, W.R., and Shaw, A.S. (2000). Signal transduction: hanging on a scaffold. *Curr. Opin. Cell Biol.* 12, 211–216.
- Chen, M.T., and Weiss, R. (2005). Artificial cell-cell communication in yeast *Saccharomyces cerevisiae* using signaling elements from *Arabidopsis thaliana*. *Nat. Biotechnol.* 23, 1551–1555.
- Chen, R.E., and Thorne, J. (2005). System biology approaches in cell signaling research. *Genome Biol.* 6, 235.
- Cullen, P.J., and Sprague, G.F., Jr. (2000). Glucose depletion causes haploid invasive growth in yeast. *Proc. Natl. Acad. Sci. USA* 97, 13619–13624.
- Dwyer, M.A., Looger, L.L., and Hellinga, H.W. (2003). Computational design of a Zn²⁺ receptor that controls bacterial gene expression. *Proc. Natl. Acad. Sci. USA* 100, 11255–11260.
- Elion, E.A. (2001). The Ste5p scaffold. *J. Cell Sci.* 114, 3967–3978.
- Ferrell, J.E. (1996). Tripping the switch fantastic: how a protein kinase cascade can convert graded inputs into switch-like outputs. *Trends Biochem. Sci.* 21, 460–466.
- Ferrell, J.E. (1997). How responses get more switch-like as you move down a protein kinase cascade. *Trends Biochem. Sci.* 22, 288–289.

- Ferrell, J.E., and Machleder, E.M. (1998). The biochemical basis of an all-or-none cell fate switch in *Xenopus* oocytes. *Science* 280, 895–898.
- Ferrell, J.E., and Xiong, W. (2001). Bistability in cell signaling: How to make continuous processes discontinuous, and reversible processes irreversible. *Chaos* 11, 227–236.
- Gao, X.D., Caviston, J.P., Tcheperegine, S.E., and Bi, E. (2004). Pxl1p, a paxillin-like protein in *Saccharomyces cerevisiae*, may coordinate Cdc42p and Rho1p functions during polarized growth. *Mol. Biol. Cell* 15, 3977–3985.
- Ghaemmaghami, S., Huh, W.K., Bower, K., Howson, R.W., Belle, A., Dephoure, N., O’Shea, E.K., and Weissman, J.S. (2003). Global analysis of protein expression in yeast. *Nature* 425, 737–741.
- Goldbeter, A., and Koshland, D.E. (1981). An amplified sensitivity arising from covalent modification in biological systems. *Proc. Natl. Acad. Sci. USA* 78, 6840–6844.
- Grunberg, R., Ferrar, T.S., van der Sloot, A.M., Constante, M., and Serrano, L. (2010). Building blocks for protein interaction devices. *Nucleic Acids Res.* 38, 2645–2662.
- Hao, N., Nayak, S., Behar, M., Shanks, R., Nagiec, M., Errede, B., Hasty, J., Elston, T., and Dohlmans, H. (2008). Regulation of Cell Signaling Dynamics by the Protein Kinase-Scaffold Ste5. *Mol. Cell* 30, 649–656.
- Harding, A., Tian, T., Westbury, E., Frische, E., and Hancock, J.F. (2005). Subcellular localization determines MAP kinase signal output. *Curr. Biol.* 15, 869–873.
- Hartwell, L.H., Hopfield, J.J., Leibler, S., and Murray, A.W. (1999). From molecular to modular cell biology. *Nature* 402, C47–C52.
- Hasty, J., McMillen, D., and Collins, J. (2002). Engineered gene circuits. *Nature* 420, 224–230.
- Heinrich, R., Neel, B.G., and Rapoport, T.A. (2002). Mathematical models of protein kinase signal transduction. *Mol. Cell* 9, 957–970.
- Hornberg, J.J., Bruggeman, F.J., Binder, B., Geest, C.R., de Vaate, A.J., Lankelma, J., Heinrich, R., and Westerhoff, H.V. (2005). Principles behind the multifarious control of signal transduction. ERK phosphorylation and kinase/phosphatase control. *FEBS J.* 272, 244–258.
- Huang, C.Y., and Ferrell, J.E. (1996). Ultrasensitivity in the mitogen-activated protein kinase cascade. *Proc. Natl. Acad. Sci. USA* 93, 10078–10083.
- Ishibe, S., Joly, D., Zhu, X., and Cantley, L.G. (2003). Phosphorylation-dependent paxillin-ERK association mediates hepatocyte growth factor-stimulated epithelial morphogenesis. *Mol. Cell* 12, 1275–1285.
- Jung, U.S., Sobering, A.K., Romeo, M.J., and Levin, D.E. (2002). Regulation of the yeast Rlm1 transcription factor by the Mpk1 cell wall integrity MAP kinase. *Mol. Microbiol.* 46, 781–789.
- Khalil, A.S., and Collins, J.J. (2010). Synthetic biology: applications come of age. *Nat. Rev. Genet.* 11, 367–379.
- Kiel, C., and Serrano, L. (2009). Cell type-specific importance of ras-c-raf complex association rate constants for MAPK signaling. *Sci. Signal.* 2, ra38.
- Kiel, C., Yus, E., and Serrano, L. (2010). Engineering signal transduction pathways. *Cell* 140, 33–47.
- Kolch, W. (2005). Coordinating ERK/MAPK signalling through scaffolds and inhibitors. *Nat. Rev. Mol. Cell Biol.* 6, 827–837.
- Levchenko, A., Bruck, J., and Sternberg, P.W. (2000). Scaffold proteins may biphasically affect the levels of mitogen-activated protein kinase signaling and reduce its threshold properties. *Proc. Natl. Acad. Sci. USA* 97, 5818–5823.
- Locasale, J.W., Shaw, A.S., and Chakraborty, A.K. (2007). Scaffold proteins confer diverse regulatory properties to protein kinase cascades. *Proc. Natl. Acad. Sci. USA* 104, 13307–13312.
- Looger, L.L., Dwyer, M.A., Smith, J.J., and Hellinga, H.W. (2003). Computational design of receptor and sensor proteins with novel functions. *Nature* 423, 185–190.
- Mackeigan, J.P., Murphy, L.O., Dimitri, C.A., and Blenis, J. (2005). Graded mitogen-activated protein kinase activity precedes switch-like c-Fos induction in mammalian cells. *Mol. Cell Biol.* 25, 4676–4682.
- Madhani, H.D., and Fink, G.R. (1997). Combinatorial control required for the specificity of yeast MAPK signaling. *Science* 275, 1314–1317.
- Marshall, C.J. (1995). Specificity of receptor tyrosine kinase signaling: transient versus sustained extracellular signal-regulated kinase activation. *Cell* 80, 179–185.
- McMahon, M. (2001). Steroid receptor fusion proteins for conditional activation of Raf-MEK-ERK signaling pathway. *Methods Enzymol.* 332, 401–417.
- Natarajan, M., Lin, K., Hsueh, R., Sternweis, P., and Ranganathan, R. (2006). A global analysis of cross-talk in a mammalian cellular signalling network. *Nat. Cell Biol.* 8, 571–580.
- Ohren, J.F., Chen, H., Pavlovsky, A., Whitehead, C., Zhang, E., Kuffa, P., Yan, C., McConnell, P., Spessard, C., Banotai, C., et al. (2004). Structures of human MAP kinase kinase 1 (MEK1) and MEK2 describe novel noncompetitive kinase inhibition. *Nat. Struct. Mol. Biol.* 11, 1192–1197.
- Poritz, M.A., Malmstrom, S., Kim, M.K., Rossmeliss, P.J., and Kamb, A. (2001). Graded mode of transcriptional induction in yeast pheromone signalling revealed by single-cell analysis. *Yeast* 18, 1331–1338.
- Qi, M. (2005). MAP kinase pathways. *J. Cell Sci.* 118, 3569–3572.
- Santos, S.D., Verveer, P.J., and Bastiaens, P.I. (2007). Growth factor-induced MAPK network topology shapes Erk response determining PC-12 cell fate. *Nat. Cell Biol.* 9, 324–330.
- Sprinzak, D., and Elowitz, M. (2005). Reconstruction of genetic circuits. *Nature* 438, 443–448.
- Whitehurst, A., Cobb, M.H., and White, M.A. (2004). Stimulus-coupled spatial restriction of extracellular signal-regulated kinase 1/2 activity contributes to the specificity of signal-response pathways. *Mol. Cell Biol.* 24, 10145–10150.
- Wu, J.J., Zhang, L., and Bennett, A.M. (2005). The noncatalytic amino terminus of mitogen-activated protein kinase phosphatase 1 directs nuclear targeting and serum response element transcriptional regulation. *Mol. Cell Biol.* 25, 4792–4803.
- Xiong, W., and Ferrell, J. (2003). A positive-feedback-based bistable ‘memory module’ that governs a cell fate decision. *Nature* 426, 460–465.
- Zhao, Y., and Zhang, Z.Y. (2001). The mechanism of dephosphorylation of extracellular signal-regulated kinase 2 by mitogen-activated protein kinase phosphatase 3. *J. Biol. Chem.* 276, 32382–32391.